Robust Control of DC-DC Boost Converters for Solar Systems

Yeqin Wang, Beibei Ren and Qing-Chang Zhong

***Abstract*—It is very challenging to control a DC-DC boost converter, due to its non-minimum phase phenomenon, model uncertainties (e.g., the parasitics), and external disturbances (e.g., input voltage change or load change). In this paper, a uncertainty and disturbance estimator (UDE)-based current-mode control (CMC) is proposed to address these problems. A new voltage dynamics is developed to avoid the non-minimum phase phenomenon. Then the UDE algorithm is adopted for both voltage-loop control design and current-loop control design to deal with model uncertainties, external disturbances, and the inductor current estimation error. Furthermore, a new control framework based on this UDE-based CMC is proposed for the grid integration of solar systems with voltage protection. Experimental results are provided to demonstrate the effectiveness and robustness of the proposed strategies.**

I. Introduction

DC-DC converter is one type of power processing devices to change the voltage level of DC sources, which has broad industrial applications in renewable energies (e.g. solar power, fuel cells), electrical vehicles, and consumer electronics (e.g. computer peripheral, adapters) [1]. A DC-DC boost converter is also called a step-up converter because the output voltage is higher than the input voltage. The boost converter has received wide attention by numerous experts and scholars with its inherited control difficulties, such as, the boost converters are highly nonlinear [2], [3], [4], [5], discontinuous in time [2], and variable structure systems [2], [6], also exhibit the non-minimum phase phenomenon [7], [3], [5], [8], [9], [10], or the right-half-plane-zero characteristic [10], [11], [12], [13]. The boost converter should have good output voltage regulation with both dynamic and steady voltage tracking performance in the presence of variations or uncertainties of system parameters [5], [14], and external disturbances with input voltage change or load change [9], [11], [14], [15]. The designed parameters for the controller are non-optimal for large disturbances [13], as the controller is designed at a particular operating point.

Because of the non-minimum phase phenomenon or the inverse response existing in the voltage dynamics of the boost converter, the voltage dynamics is not directly used for controller design, and even is often omitted, e.g. in [14], [16], [17], [18]. Therefore, the current-mode control (CMC) methods are widely used for the control of the boost converter with an external voltage-loop and an inner current-loop, e.g. in [8], [14], [15], [19]. Most CMCs focus on the design of current-loop. For example, an exponential form of linear multi-loop controller is proposed in [15] to modify the output response with the additional tuning parameters. Nonlinear CMC is proposed in [20] to eliminate the sensitivity of the control-to-output transfer function. A robust inner-loop current controller is embedded in [14] against parameter variations. An adaptive ramp CMC is proposed in [21] to suppress chaos and subharmonic oscillations for a wide range of input voltage and load values. Though CMC has many advantages, such as faster transient response induced by the current-loop, an easier-to-design control loop, and faster overload protection, as well as its ability to deal with practical variations on circuit parameters and line voltage [15], the proportional-integral (PI) algorithm is still required to eliminate modeling error and current estimation error for voltage-loop control in these designs, e.g. in [14], [21]. Furthermore, the theoretical analysis of the cascade controller with PI and sliding-mode control (SMC) for a boost converter has been investigated in [4] to show the stability and robustness of the closed-loop system.

Other one-loop control methods for the DC-DC boost converter can be seen in [11], [12], [17] etc. H^{∞}control is applied to deal with the right-half-plane zero in the transfer function from the duty cycle to the output voltage [11]. A fixed-frequency SMC is proposed in [12] to achieve a faster response and a lower voltage overshoot over a wide range of operating conditions. Sensorless current mode integral control is proposed to carry over output error and handle large load disturbances [17], but a PI control loop for voltage regulation is still needed to compensate the effects of the parasitics. A new control algorithm that combines a proportional-integral-differential (PID) controller with the parallel-damped passivity-based controller (PBC) is proposed to achieve robust output regulation against load uncertainties [5]. An adaptive interconnection and damping assignment (IDA)-PBC is proposed in [22] with the similar complementary PI controller. A robust adaptive sliding-mode controller is designed for a boost converter with an asymptotically stable closed-loop system [6]. A geometric pulse-width modulation (PWM) strategy is introduced in [16] with the similar idea of SMC. A H_{∞} type performance criterion with integral action and average sampling is proposed in [23] to provide robustness against plant uncertainty. Another trend for robust control of DC-DC boost converters is with discontinuous conduction mode (DCM), e.g. with predictive current control

Yeqin Wang is with the National Wind Institute, Texas Tech University, Lubbock, TX 79409-1021, USA. (e-mail: yeqin.wang@ttu.edu).

Beibei Ren is with the Department of Mechanical Engineering, Texas Tech University, Lubbock, TX 79409-1021, USA. (e-mail: beibei.ren@ttu.edu).

Qing-Chang Zhong is with the Department of Electrical and Computer Engineering, Illinois Institute of Technology, Chicago, IL 60616, USA. (e-mail: zhongqc@ieee.org).

(PCC) method, [3], [24], [25], [26], [27], with boundary control [13], or with hybrid control [28]. However, DCM control requires a lot of calculation resources to regulate the current in every switching cycle, and, the PI algorithm is still required to for voltage-loop control in these designs, e.g. in [3], [24], [26].

Sensorless control can provide system reliability and reduce system cost. Many estimation technologies are proposed for the DC-DC boost converter. For example, a sensorless explicit model predictive control with coil current estimation via a static approximation and an extended Kalman filter is presented in [3]. A time-domain inductor current estimation is designed in [29] with a discrete-time low-pass filter in each switching cycle borrowing the idea from [25]. Similar current estimation idea is still adopted in [24], [26]. A state observer is presented in [30] dedicated to online estimation. However, the estimation error still affects the accuracy of voltage regulation of the boost converter [18]. Therefore, the PI control for voltage-loop or extra integral of voltage error is usually adopted for the compensation of estimation error.

Though a lot of research activities have been done for the DC-DC boost converter control, the PI control or integral control for voltage-loop is still required because of its non-minimum phase phenomenon. In this paper, a new voltage dynamics is proposed to avoid the non-minimum phase phenomenon. A uncertainty and disturbance estimator (UDE)-based CMC is proposed for the control of the DC-DC boost converter. The UDE technology is originally proposed in [31] wherein the modeling uncertainties and system disturbances are estimated and compensated by an appropriate filter. In recent years, the UDE strategy has been further elaborated in [32], [33], [34], [35] and broadly applied to different applications, such as robust trajectory tracking [36], variable-speed wind turbine control [37], and power inverter control [38], [39], etc. In this paper, the UDE-based method is adopted in both voltage-loop control and current-loop control to deal with model uncertainties, external disturbances, and the inductor current estimation error to achieve the voltage and current regulation, respectively.

Also, it is known that robust voltage control of the DC-DC boost converter is very important for the solar application. However, the output voltage of the boost converter, also called DC bus voltage, is usually regulated by the grid-connected inverter, while the maximum power point tracking (MPPT) function is usually embedded into the control of the DC-DC boost converter for grid-connected solar systems [40], [41], [42]. In this case, if some faults happen to the grid side or the grid-connected inverter, the DC bus voltage will increase due to the continuous operation of the DC-DC boost converter with MPPT. Then the power electronic device might be broken down due to the high DC bus voltage, as well as the PV source. In this paper, a new control framework is proposed for the grid integration of solar systems with the DC bus voltage controlled by the DC-DC converter and the MPPT function embedded into the grid-connected inverter. This naturally provides the DC bus voltage protection, because the DC bus voltage is always regulated even in the fault conditions of grid side or the grid-connected inverter. The effectiveness of the proposed control strategies are demonstrated through experimental studies on an experimental test rig, which consists of a Texas Instruments (TI) solar explorer kit delivering power to a grid simulator.

The rest of this paper is organized as follows. Section II provides the dynamics of the DC-DC boost converter. In Section III, the UDE-based CMC is proposed before the application of solar systems in Section IV. Effectiveness of the proposed approach is demonstrated through experimental studies in Section V, followed by the concluding remarks in Section VI.

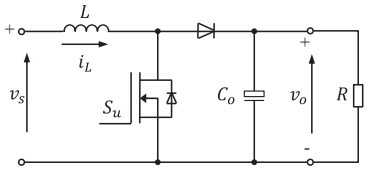

Figure 1. The DC-DC boost converter.

II. Dynamics of DC-DC boost converter

A. Nominal dynamics of DC-DC boost converter

As shown in Fig. 1, the nominal dynamics of the DC-DC boost converter without the parasitics can be modeled as

$$\dot{v}_o = (1-u)\frac{i_L}{C_o} - \frac{v_o}{RC_o}, \tag{1}$$

$$\dot{i}_L = -(1-u)\frac{v_o}{L} + \frac{v_s}{L}. \tag{2}$$

where v_o is the output voltage of the boost converter, i_L is inductor current. The L and C_o are the inductance of the inductor, the capacitance of the output capacitor, respectively. R is load resistance, which can be a real resistance from a resistor load or a virtual resistance estimated by other parameters. u is the duty cycle of a pulse-width modulation (PWM) control signal S_u for power electronic device within the range of 0~100%. v_s is the input voltage. Furthermore, the model of this DC-DC boost converter can be rewrittenas

$$\dot{v}_o = -\frac{1}{RC_o}v_o + \frac{1}{C_o}i_L - \frac{1}{C_o}i_L u, \tag{3}$$

$$\dot{i}_L = -\frac{1}{L}v_o + \frac{1}{L}v_o u + \frac{v_s}{L}. \tag{4}$$

The detailed analysis about the non-minimum phase phenomenon of this boost converter can be seen [8], [11]. Also, for the DC-DC boost converter, the averaged relationship between input voltage and output voltage is given as

$$v_o = \frac{v_s}{1-u},$$

which indicates the output voltage v_o has a positive correlation with system input u. However, the term $-\frac{1}{C_o}i_L u$ in voltage dynamics (3) is an inverse response with $\frac{1}{C_o}i_L > 0$. Because of the non-minimum phase phenomenon or the inverse response, the voltage dynamics (3) is usually not directly used for the controller design, and even is often omitted.

B. Revised dynamics of DC-DC boost converter

In this paper, a new voltage dynamics is proposed to avoid the non-minimum phase phenomenon or the inverse response. By setting $\dot{v}_o = 0$ in (3) and $\dot{i}_L = 0$ in (4), it is easy to obtain

$$v_o^2 = v_s R i_L, \tag{5}$$

which is a power balance equation in the steady state with the input power $v_s i_L$ equal to the output power $\frac{v_o^2}{R}$ without considering the losses of components and parasitics.

To facilitate the controller design, following the method with filter dynamics in [39], a first-order filter is introduced on the right hand side of (5),

$$v_o^2 = \mathcal{L}^{-1}\left\{\frac{1}{1+\tau_{sv}s}\right\} * v_s R i_L, \tag{6}$$

or,

$$\dot{v}_o = \frac{v_s R}{2\tau_{sv} v_o} i_L - \frac{v_o}{2\tau_{sv}}, \tag{7}$$

where " $*$ " is the convolution operator, and $\mathcal{L}^{-1}$ means the inverse Laplace transformation.

The revised dynamics of the DC-DC boost converter can be rewritten as

$$\dot{v}_o = \frac{v_s R}{2\tau_{sv} v_o} i_L - \frac{v_o}{2\tau_{sv}} + \triangle_v, \tag{8}$$

$$\dot{i}_L = -\frac{1}{L} v_o + \frac{1}{L} v_o u + \frac{v_s}{L} + \triangle_i, \tag{9}$$

where $\triangle_v$ and $\triangle_i$ represent the uncertain terms, which include the model uncertainties (e.g., the parasitics), the effects of the losses of components, and the approximation errors caused by the introduction of the first-order filter in (6). The uncertain terms $\triangle_v$ and $\triangle_i$ will be estimated and compensated in the controller design in Section III.

III. UDE-BASED CMC

In this paper, a UDE-based CMC is developed for the DC-DC boost converter based on the revised dynamics (8) and (9). The UDE-based method is adopted in both voltage-loop and current-loop to deal with model uncertainties, external disturbances, and the inductor current estimation error.

A. Controller design

1) Voltage-loop design: The control objective is to design a virtual control input i_{ref} to make the output voltage v_o asymptotically track the voltage reference v_{ref}. The tracking error, $e_v = v_{ref} - v_o$, should satisfy the error dynamic equation

$$\dot{e}_v = -k_v e_v, \tag{10}$$

where $k_v > 0$ is a constant error feedback gain. Combining (8) and (10), then

$$\dot{v}_{ref} - \frac{v_s R}{2\tau_{sv} v_o} i_{ref} + \frac{v_o}{2\tau_{sv}} - \triangle_v = -k_v e_v,$$

Therefore, i_{ref} needs to satisfy

$$i_{ref} = \frac{2\tau_{sv} v_o}{v_s R}\left(\dot{v}_{ref} + \frac{v_o}{2\tau_{sv}} - \triangle_v + k_v e_v\right). \tag{11}$$

According to the voltage dynamics (8), the uncertain term $\triangle_v$ can be represented as

$$\triangle_v = \dot{v}_o - \frac{v_s R}{2\tau_{sv} v_o} i_{ref} + \frac{v_o}{2\tau_{sv}}.$$

Following the UDE procedures provided in [31], $\triangle_v$ can be estimated by

$$\hat{\triangle}_v = \triangle_v * g_{vf} = \left(\dot{v}_o - \frac{v_s R}{2\tau_{sv} v_o} i_{ref} + \frac{v_o}{2\tau_{sv}}\right) * g_{vf}, \tag{12}$$

where g_{vf} is the impulse response of a strictly proper stable filter $G_{vf}(s)$ with the appropriate bandwidth. Replacing $\triangle_v$ with $\hat{\triangle}_v$ in (11) results in

$$\begin{aligned} i_{ref} = {} & \frac{2\tau_{sv} v_o}{v_s R}\Bigg[\dot{v}_{ref} + \frac{v_o}{2\tau_{sv}} + k_v e_v \\ & - \left(\dot{v}_o - \frac{v_s R}{2\tau_{sv} v_o} i_{ref} + \frac{v_o}{2\tau_{sv}}\right) * g_{vf}\Bigg], \end{aligned}$$

Then, the UDE-based control law can be formulated as

$$\begin{aligned} i_{ref} = {} & \tfrac{v_o^2}{v_s R} + \frac{2\tau_{sv} v_o}{v_s R}\Bigg[\mathcal{L}^{-1}\left\{\frac{1}{1-G_{vf}(s)}\right\} \\ & * (\dot{v}_{ref} + k_v e_v) \\ & - \mathcal{L}^{-1}\left\{\frac{sG_{vf}(s)}{1-G_{vf}(s)}\right\} * v_o\Bigg]. \end{aligned} \tag{13}$$

2) Current-loop design: With i_{ref} designed in the previous subsection, the control objective in this subsection is to manipulate the duty cycle u^* such that the inductor current i_L tracks the reference signal i_{ref}. The tracking error, $e_i = i_{ref} - i_L$, still needs to satisfy

$$\dot{e}_i = -k_i e_i, \tag{14}$$

where $k_i > 0$ is a constant error feedback gain.

Combining current dynamics (9) and the desired error dynamics (14), and following the similar procedures of UDE-based control in the previous subsection, the UDE-based control law for the duty cycle u^* can be obtained as

$$\begin{aligned} u^* = {} & 1 - \frac{v_s}{v_o} + \frac{L}{v_o}\Bigg[\mathcal{L}^{-1}\left\{\frac{1}{1-G_{if}(s)}\right\} * (\dot{i}_{ref} + k_i e_i) \\ & - \mathcal{L}^{-1}\left\{\frac{sG_{if}(s)}{1-G_{if}(s)}\right\} * i_L\Bigg]. \end{aligned} \tag{15}$$

where $G_{if}(s)$ is a strictly proper stable filter with the appropriate bandwidth to cover the spectrum of uncertain term $\triangle_i$.

It is worth noting that the UDE-based control laws (13) and (15) include the derivative terms $\dot{v}_{ref}$ and $\dot{i}_{ref}$, which can be numerically approximated using the low pass filters, as discussed in [39].

3) Estimation of inductor current: In order to reduce system cost and provide system reliability, the current estimation is usually adopted instead of direct measurement for the current-loop design. To guarantee the convergence of the current estimation error, the original current dynamics (4) is revised with an additional term from the inductor parasitics,

$$\dot{i}_L = -\frac{1}{L} v_o + \frac{1}{L} v_o u^* + \frac{v_s}{L} - \frac{r_L}{L} i_L, \tag{16}$$

where r_L is the parasitics resistance and its nominal value can be measured easily. It is worth noting that the term $-\frac{r_L}{L}i_L$ is lumped into the uncertain term $\triangle_i$ in (9), which is estimated, and compensated by the UDE-based control in the current-loop design.

Then, the current estimation is designed based on the current dynamics (16) of the DC-DC boost converter. With the known output voltage v_o and the duty cycle u^*, the estimation law is designed as

$$\dot{\hat{i}}_L = -\frac{1}{L}v_o + \frac{1}{L}v_o u^* + \frac{v_s}{L} - \frac{r_L}{L}\hat{i}_L. \quad (17)$$

where $\hat{i}_L$ is the estimation of the inductor current. The discrete form of this estimation law (17) is very popular in PCC methods, e.g. in [24], [26], [29].

With the estimation error $e_{oi} = i_L - \hat{i}_L$, the error dynamics of the current estimation is obtained as

$$\dot{e}_{oi} = -\frac{r_L}{L}e_{oi}. \quad (18)$$

Solving (18) results in

$$e_{oi}(t) = e_{oi}(0)e^{-ct}, \quad (19)$$

where $c = \frac{r_L}{L} > 0$, and $e_{oi}(0)$ is the initial error. When $t \to \infty$, the estimation error $e_{oi}(t)$ will decay to 0, which achieves the convergence of the current estimation error.

In practice, the perfect estimation might not be achieved through (16) due to model uncertainties. However, the inductor current estimation error can be lumped into the uncertain term $\triangle_v$, which can be estimated through (12), and compensated by this UDE-based CMC in voltage-loop design. The related experimental results are shown in Section V.

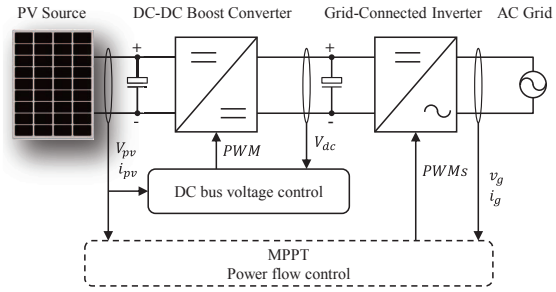

Figure 2. Solar system application.

IV. Solar system application

In this paper, a new control framework for the grid integration of solar systems is proposed as shown in Fig. 2, including a DC bus voltage control for the DC-DC boost converter, MPPT and power flow control for the grid-connected inverter. Different from the conventional framework [40], [41], [42], where the DC bus voltage is regulated by the grid-connected inverter, the UDE-based CMC is provided for the output voltage control of the DC-DC boost converter. Then, the DC bus voltage can always be regulated, even in the fault conditions of grid-connected inverter side, which makes the PV system more safe and reliable.

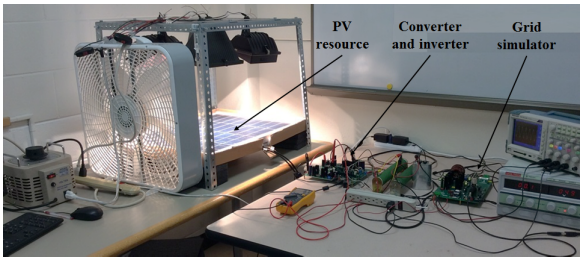

Figure 3. Experimental setup

On the grid-connected inverter side, the gradient-based extremum seeking (ES) MPPT [43] is introduced to maximize the output power of PV source. The UDE-based robust power flow control [38] is adopted to convert the DC bus power to AC grid power. Since this paper focuses on the control design for the DC-DC boost converter, the detailed information about the design of MPPT and power flow control are omitted here and can be found in [38], [43].

V. Experimental results

A. Experimental setup

To verify the proposed UDE-based CMC (13) and (15) for the DC-DC boost converter and the new control framework for solar systems in Fig. 2, a test rig with one PV system delivering power to a grid simulator as shown in Fig. 3 is built, wherein the PV system includes a solar panel, RENOGY RNG-50P, a Texas Instruments solar explorer kit including the DC-DC boost converter and the grid-connected inverter, and four 450W halogen floodlights which can be tuned by a transformer to mimic the sunlight. The detailed setup of the grid simulator can be found in [38]. The parameters of the DC-DC boost converter are listed in Table I. The parameters of the solar panel can be found in [44]. The regulation set-point of the DC bus voltage is 35V.

B. Filter design and parameter selection

The filters in the UDE algorithm should cover the spectrum of uncertainties and disturbances with the proper bandwidth. Here, $G_{vf}(s)$ and $G_{if}(s)$ are chosen as the following first-order low-pass filters

$$G_{vf}(s) = \frac{1}{1+\tau_v s}, \quad G_{if}(s) = \frac{1}{1+\tau_i s}. \quad (20)$$

The control parameters are shown in Table II. As discussed in [39], the time constant τ_{sv} in the first-order filter for new voltage dynamics should be very fast, but limited by the control sampling time, 0.0004 s. The error feedback gain of current error dynamics k_i should be smaller than the error feedback gain in current estimation $c = \frac{r_L}{L}$. The error feedback gain k_v in the voltage-loop should be smaller than k_i in the current-loop, because of the cascaded control design. The time constants τ_v and τ_i of UDE filters $G_{vf}(s)$ and $G_{if}(s)$ should be smaller than $\frac{1}{k_v}$ and $\frac{1}{k_i}$, respectively, to

fulfill the requirements from the responses of error dynamics (10) and (14), i.e., the bandwidths of UDE filters should be wide enough to cover the spectrum of the lumped uncertain terms $\triangle_v$ and $\triangle_i$, respectively.

Table I
THE PARAMETERS OF THE DC-DC .

Parameters	Values	Parameters	Values
L	100 μH	PV output capacitor	680 μF
C_o	1640 μF	PWM frequency	100 kHz
r_L	0.2 Ω	-	-

Table II
CONTROL PARAMETERS

Parameters	Values	Parameters	Values
v_{ref}	35 V	τ_v	0.01 s
τ_{sv}	0.001 s	k_i	100
k_v	10	τ_i	0.001 s

C. System performance

The system starts at $t = 0$ s. The footlights are given almost at their maximum output, and the DC-DC boost converter starts to regulate the DC bus voltage. Then the grid-connected inverter delivers a small amount of power to the simulated grid (2 W setting), and MPPT is enabled after $t = 5$ s. At $t = 150$ s, the floodlights are tuned to about half of their maximum output, and back to the maximum at $t = 200$ s. The system stops at $t = 300$ s.

The system responses are shown in Fig. 4, including DC bus voltage in Fig. 4(a), PV output voltage in Fig. 4(b). The real power output and reactive power output of the grid-connected inverter are shown in Fig. 4(c) and in Fig. 4(d), respectively. Initially, the DC bus voltage is regulated to its set-point $v_o = 35$ V quickly. After enabling MPPT, the real power output goes up to the maximum value within 50 s, and the PV output voltage drops correspondingly. At $t = 150$ s, the output power drops quickly with half of maximum output of floodlights, and PV voltage also drops. At $t = 200$ s, the PV voltage goes up, as the floodlights are given at their maximum output. The output real power achieves the maximum value again within 30 s. The reactive power output almost keeps 0 Var through the whole experimental stage. It is worth noting that both the PV output voltage and real power output drop slowly during the steady states. The reason is that the temperature of the solar panel increases slowly with high irradiation of the floodlights. It can be seen that the DC bus voltage always keeps at the set-point value well during the whole experiment. Therefore, the UDE-based CMC has good robustness to regulate DC bus voltage in the presence of model uncertainties, external disturbances (the change of PV output voltage, and load change), and the inductor current estimation error.

VI. CONCLUSION

In this paper, a UDE-based CMC has been proposed for the DC-DC boost converter to achieve robust output voltage regulation. A new voltage dynamics has been introduced to deal with non-minimum phase phenomenon. Then the UDE algorithm has been adopted for both voltage-loop design and current-loop design to deal with model uncertainties, external disturbances, and the inductor current estimation error. The effectiveness of the proposed UDE-based CMC has been experimentally validated in the grid integration of the solar system with a new control framework.

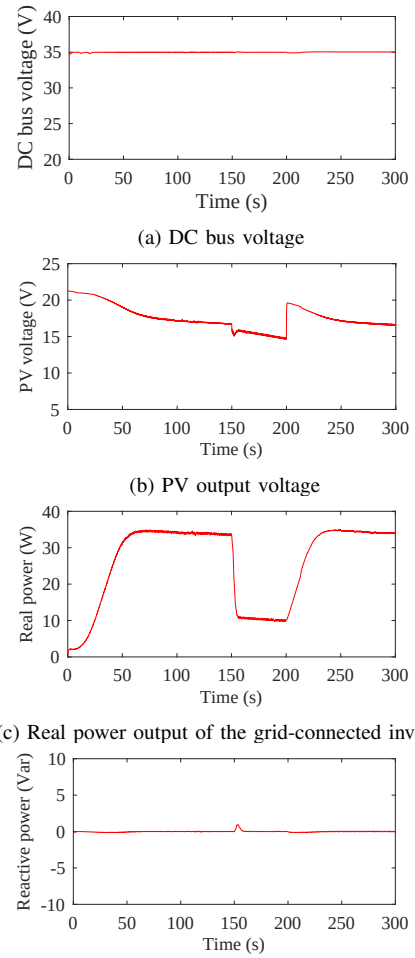

(a) DC bus voltage

(b) PV output voltage

(c) Real power output of the grid-connected inverter

(d) Reactive power output of the grid-connected inverter

Figure 4. Experimental results

ACKNOWLEDGMENT

The authors would like to thank Texas Instruments for the donation of the inverter kit TMDSHV1PHINVKIT.

REFERENCES

[1] Q.-C. Zhong and T. Hornik, *Control of Power Inverters in Renewable Energy and Smart Grid Integration*. Wiley-IEEE Press, 2013.

[2] C. Sreekumar and V. Agarwal, "A hybrid control algorithm for voltage regulation in DC-DC boost converter," *IEEE Trans. Ind. Electron.*, vol. 55, no. 6, pp. 2530–2538, Jun. 2008.

[3] A. Beccuti, S. Mariethoz, S. Cliquennois, S. Wang, and M. Morari, "Explicit model predictive control of DC-DC switched-mode power supplies with extended Kalman filtering," *IEEE Trans. Ind. Electron.*, vol. 56, no. 6, pp. 1864–1874, Jun. 2009.

[4] Z. Chen, W. Gao, J. Hu, and X. Ye, "Closed-loop analysis and cascade control of a nonminimum phase boost converter," *IEEE Trans. Power Electron.*, vol. 26, no. 4, pp. 1237–1252, 2011.

[5] Y. I. Son and I. H. Kim, "Complementary PID controller to passivity-based nonlinear control of boost converters with inductor resistance," *IEEE Trans. Control Syst. Technol.*, vol. 20, no. 3, pp. 826–834, May 2012.

[6] S. Oucheriah and L. Guo, "PWM-based adaptive sliding-mode control for boost DC–DC converters," *IEEE Trans. Ind. Electron.*, vol. 60, no. 8, pp. 3291–3294, 2013.

[7] H. Rodriguez, R. Ortega, G. Escobar, and N. Barabanov, "A robustly stable output feedback saturated controller for the boost DC-to-DC converter," *Systems & Control Letters*, vol. 40, no. 1, pp. 1–8, 2000.

[8] J. Alvarez-Ramirez, G. Espinosa-Perez, and D. Noriega-Pineda, "Current-mode control of DC-DC power converters: A backstepping approach," in *Proc. IEEE Int. CCA*, Sept. 2001, pp. 190–195.

[9] J. Linares-Flores, A. H. Mendez, C. Garcia-Rodriguez, and H. Sira-Ramirez, "Robust nonlinear adaptive control of a "boost" converter via algebraic parameter identification," *IEEE Trans. Ind. Electron.*, vol. 61, no. 8, pp. 4105–4114, Aug. 2014.

[10] I. G. Zurbriggen and M. Ordonez, "Benchmarking the performance of boost-derived converters under start-up and load transients," *IEEE Trans. Ind. Electron.*, vol. 63, no. 5, pp. 3125–3136, May 2016.

[11] R. Naim, G. Weiss, and S. Ben-Yaakov, "H^∞ control applied to boost power converters," *IEEE Trans. Power Electron.*, vol. 12, no. 4, pp. 677–683, Jul. 1997.

[12] S.-C. Tan, Y. M. Lai, C. K. Tse, L. Martinez-Salamero, and C.-K. Wu, "A fast-response sliding-mode controller for boost-type converters with a wide range of operating conditions," *IEEE Trans. Ind. Electron.*, vol. 54, no. 6, pp. 3276–3286, Dec. 2007.

[13] T.-T. Song and H. S.-H. Chung, "Boundary control of boost converters using state-energy plane," *IEEE Trans. Power Electron.*, vol. 23, no. 2, pp. 551–563, Mar. 2008.

[14] S.-K. Kim and K.-B. Lee, "Robust feedback-linearizing output voltage regulator for DC/DC boost converter," *IEEE Trans. Ind. Electron.*, vol. 62, no. 11, pp. 7127–7135, Nov. 2015.

[15] C.-Y. Chan, "A nonlinear control for DC-DC power converters," *IEEE Trans. Power Electron.*, vol. 22, no. 1, pp. 216–222, Jan. 2007.

[16] I. G. Zurbriggen, M. Ordonez, and M. Anun, "PWM-geometric modeling and centric control of basic DC-DC topologies for sleek and reliable large-signal response," *IEEE Trans. Ind. Electron.*, vol. 62, no. 4, pp. 2297–2308, Apr. 2015.

[17] P. Midya, P. T. Krein, and M. F. Greuel, "Sensorless current mode control-an observer-based technique for DC-DC converters," *IEEE Trans. Power Electron.*, vol. 16, no. 4, pp. 522–526, Jul. 2001.

[18] R. Min, Q. Tong, Q. Zhang, X. Zou, K. Yu, and Z. Liu, "Digital sensorless current mode control based on charge balance principle and dual current error compensation for DC-DC converters in DCM," *IEEE Trans. Ind. Electron.*, vol. 63, no. 1, pp. 155–166, Jan. 2016.

[19] O. Lopez-Santos, L. Martinez-Salamero, G. Garcia, H. Valderrama-Blavi, and T. Sierra-Polanco, "Robust sliding-mode control design for a voltage regulated quadratic boost converter," *IEEE Trans. Power Electron.*, vol. 30, no. 4, pp. 2313–2327, Apr. 2015.

[20] S. Hiti and D. Borojevic, "Robust nonlinear control for boost converter," *IEEE Trans. Power Electron.*, vol. 10, no. 6, pp. 651–658, Nov. 1995.

[21] J. D. Morcillo, D. Burbano, and F. Angulo, "Adaptive ramp technique for controlling chaos and subharmonic oscillations in DC-DC power converters," *IEEE Trans. Power Electron.*, vol. 31, no. 7, pp. 5330–5343, Jul. 2016.

[22] J. Zeng, Z. Zhang, and W. Qiao, "An interconnection and damping assignment passivity-based controller for a DC-DC boost converter with a constant power load," *IEEE Trans. Ind. Appl.*, vol. 50, no. 4, pp. 2314–2322, Jul. 2014.

[23] H. Fujioka, C.-Y. Kao, S. Almer, and U. Jonsson, "Robust tracking with H_∞ performance for PWM systems," *Automatica*, vol. 45, no. 8, pp. 1808–1818, Aug. 2009.

[24] Q. Tong, Q. Zhang, R. Min, X. Zou, Z. Liu, and Z. Chen, "Sensorless predictive peak current control for boost converter using comprehensive compensation strategy," *IEEE Trans. Ind. Electron.*, vol. 61, no. 6, pp. 2754–2766, Jun. 2014.

[25] J. Chen, A. Prodic, R. W. Erickson, and D. Maksimovic, "Predictive digital current programmed control," *IEEE Trans. Power Electron.*, vol. 18, no. 1, pp. 411–419, Jan. 2003.

[26] Z. Shen, X. Chang, W. Wang, X. Tan, N. Yan, and H. Min, "Predictive digital current control of single-inductor multiple-output converters in CCM with low cross regulation," *IEEE Trans. Power Electron.*, vol. 27, no. 4, pp. 1917–1925, Apr. 2012.

[27] Q. Zhang, R. Min, Q. Tong, X. Zou, Z. Liu, and A. Shen, "Sensorless predictive current controlled DC-DC converter with a self-correction differential current observer," *IEEE Trans. Ind. Electron.*, vol. 61, no. 12, pp. 6747–6757, Dec. 2014.

[28] T. A. F. Theunisse, J. Chai, R. G. Sanfelice, and W. P. M. H. Heemels, "Robust global stabilization of the DC-DC boost converter via hybrid control," *IEEE Trans. Circuits Syst. I: Reg. Papers*, vol. 62, no. 4, pp. 1052–1061, April 2015.

[29] Y. Qiu, H. Liu, and X. Chen, "Digital average current-mode control of PWM DC-DC converters without current sensors," *IEEE Trans. Ind. Electron.*, vol. 57, no. 5, pp. 1670–1677, May 2010.

[30] H. Renaudineau, J. P. Martin, B. Nahid-Mobarakeh, and S. Pierfederici, "DC-DC converters dynamic modeling with state observer-based parameter estimation," *IEEE Trans. Power Electron.*, vol. 30, no. 6, pp. 3356–3363, Jun. 2015.

[31] Q.-C. Zhong and D. Rees, "Control of uncertain LTI systems based on an uncertainty and disturbance estimator," *Journal of Dyn. Sys. Meas. Con.Trans. ASME*, vol. 126, no. 4, pp. 905–910, Dec. 2004.

[32] B. Ren, Q.-C. Zhong, and J. Chen, "Robust control for a class of non-affine nonlinear systems based on the uncertainty and disturbance estimator," *IEEE Trans. Ind. Electron.*, vol. 62, no. 9, pp. 5881–5888, Sept. 2015.

[33] B. Ren, Q.-C. Zhong, and J. Dai, "Asymptotic reference tracking and disturbance rejection of UDE-based robust control," *IEEE Trans. Ind. Electron.*, 2016, DOI 10.1109/TIE.2016.2633473.

[34] L. Sun, D. Li, Q. C. Zhong, and K. Y. Lee, "Control of a class of industrial processes with time delay based on a modified uncertainty and disturbance estimator," *IEEE Trans. Ind. Electron.*, vol. 63, no. 11, pp. 7018–7028, Nov. 2016.

[35] S. E. Talole, T. S. Chandar, and J. P. Kolhe, "Design and experimental validation of UDE based controller-observer structure for robust input-output linearisation," *International Journal of Control*, vol. 84, no. 5, pp. 969–984, 2011.

[36] J. P. Kolhe, M. Shaheed, T. S. Chandar, and S. E. Taloe, "Robust control of robot manipulators based on uncertainty and diturbance estimation," *International Journal of Robust and Nonlinear Control*, vol. 23, no. Jan., pp. 104–122, 2013.

[37] B. Ren, Y. Wang, and Q.-C. Zhong, "UDE-based control of variable-speed wind turbine systems," *International Journal of Control*, vol. 90, no. 1, pp. 137–152, 2015.

[38] Y. Wang, B. Ren, and Q.-C. Zhong, "Robust power flow control of grid-connected inverters," *IEEE Trans. Ind. Electron.*, vol. 63, no. 11, pp. 6887–6897, Nov. 2016.

[39] Q.-C. Zhong, Y. Wang, and B. Ren, "UDE-based robust droop control of inverters in parallel operation," *IEEE Trans. Ind. Electron.*, 2017, accepted.

[40] N. Femia, G. Petrone, G. Spagnuolo, and M. Vitelli, "Optimization of perturb and observe maximum power point tracking method," *IEEE Trans. Power Electron.*, vol. 20, no. 4, pp. 963–973, Jul. 2005.

[41] D. G. Montoya, C. A. Ramos-Paja, and R. Giral, "Improved design of sliding-mode controllers based on the requirements of MPPT techniques," *IEEE Trans. Power Electron.*, vol. 31, no. 1, pp. 235–247, Jan. 2016.

[42] Y. Shi, R. Li, Y. Xue, and H. Li, "High-frequency-link-based grid-tied PV system with small DC-link capacitor and low-frequency ripple-free maximum power point tracking," *IEEE Trans. Power Electron.*, vol. 31, no. 1, pp. 328–339, Jan. 2016.

[43] A. Ghaffari, M. Krstic, and S. Seshagiri, "Power optimization for photovoltaic microconverters using multivariable newton-based extremum seeking," *IEEE Trans. Control Syst. Technol.*, vol. 22, no. 6, pp. 2141–2149, Nov. 2014.

[44] 50 W polycrystalline solar panel. [Online]. Available: https://www.renogy.com/template/files/Specifications/50-Watt-12-Volt-Polycrystalline-Solar-Panel-Specifications.pdf